Final Draft
of the original manuscript:

Reimann, M.; Goebel, J.; Gartner, T.M.; dos Santos, J.F.:
Refilling termination hole in AA 2198–T851 by refill friction stir spot welding

In: Journal of Materials Processing Technology (2017) Elsevier

DOI: 10.1016/j.jmatprotec.2017.02.025

Refilling termination hole in AA 2198–T851 by refill friction stir spot welding

Authors:

Martin Reimann[a], Jannik Goebel[a], Thomas M. Gartner[b], Jorge F. dos Santos[a]

Affiliations:

[a] Helmholtz-Zentrum Geesthacht, Institute of Materials Research, Materials Mechanics, Solid State Joining Processes Department, Max-Planck-Str. 1, 21502 Geesthacht, Germany

[b] Innovation Management and Product Development, Lufthansa Technik AG, Weg beim Jäger 193, 22335 Hamburg, Germany

Corresponding author:

Martin Reimann. Tel.: +49 4152 872073 fax: +49 4152 2033 mail: martin.reimann@hzg.de

Abstract

Friction stir welding features a joining technology with only few drawbacks. The exit hole inevitably left by the tool is a major disadvantage. In order to eliminate volume defects such as termination holes or voids in friction stir welds, refill friction stir spot welding was used for keyhole repair. The keyhole closure process was employed to 3 mm thick sheets of aluminum-lithium alloy AA 2198-T851. Exit holes with a diameter of 7.5 mm in semi–stationary shoulder bobbin tool friction stir welds were refilled successfully.

To characterize the refilling process characteristic process parameters such as position, force and torque of the tool parts have been monitored. The welds have been analyzed with regards to microstructural features, the local and global mechanical performance as well as the thermal cycle. The properties of the repair welds have been compared to friction stir welded butt joints and keyhole closure welds in bare sheet.

A systematic investigation comparing and combining the two friction based processes has shown that refill friction stir spot welding is able to be applied as keyhole closure technique in sheet material and in semi–stationary shoulder bobbin tool friction stir welds. Defect free welds with known microstructural features were achieved. The mechanical performance of keyhole closure welds using refill friction stir spot welding in semi–stationary shoulder bobbin tool friction stir welds is comparable to the performance of keyhole closure welds in bare sheets. High-strength keyhole closure welds with efficiencies of 78 % in terms of ultimate tensile strength were achieved.

Keywords

friction spot welding; keyhole closure; BT-FSW, aluminum–lithium alloy, AA 2198

1 Introduction

Friction stir welding (FSW) is well known and has shown superior capabilities when welding lightweight materials such as aluminum. Bobbin tool friction stir welding (BT-FSW) is a variant of the solid-state process friction stir welding. The principle of BT-FSW is identical to FSW by means of forming a strong joint by intermixing plasticized material. The main difference between the processes is that the frictional heat is applied from two sides in BT-FSW, as the tool, in this case, consists of two rotating shoulders connected by a probe as stated by Goebel et al. (2016). In recent years, the stationary shoulder developed in FSW tools was applied in the BT-FSW process to further reduce the total heat input. Although a fully stationary BT-FSW process has shown challenges in terms of tool material and design, the concept of using one stationary shoulder has been proved. The upper shoulder was decoupled and held stationary while the probe and the lower shoulder remained rotating. This semi–stationary shoulder bobbin tool friction stir welding process with a stationary upper shoulder (SS_UBT-FSW) was recently presented by Goebel et al. (2016), who successfully welded the aluminum-lithium alloy 2198–T851. Aluminum-lithium alloys are of special interest when highly specific strength and stiffness are required owing to the contribution of lithium to reduce the density and enhance the elastic modulus and strength (Giummarra et al., 2007). The results were promising, with joint efficiencies of 82% in terms of tensile strength and 71% in hardness. Compared with a previous study by Wang et al. (2015) who used conventional BT-FSW on the same alloy, the SS_UBT -FSW process showed improvements in mechanical performance and applicability.

The BT-FSW process variant is particularly suitable for closed structures such as pipes or hollow structures. A major drawback of the BT-FSW process is the remaining exit hole at the end of the weld resulting from the extraction of the welding tool. A process dealing with this issue has to be chosen when employing the technique in industrial products. In some applications, the question of the keyhole closure can be avoided by creating a runoff plate that can be removed after the welding. Due to the lower shoulder connected to the probe, this is not possible when welding hollow structures with BT–FSW. In conventional FSW, there are some approaches to avoid the exit hole including the retractable pin developed by Ding and Oelgoetz (1996). A double-acting tool consisting of an outer shoulder and inner probe is used incrementally to retract the probe in the final stages of the FSW process. This approach is inapplicable to the BT-FSW process owing to the two-shoulder design.

Aluminum lithium alloys are difficult to weld through conventional fusion welding methods as summarized by Çam and Koçak (1998). They concluded that fusion welding in Al-Li alloys usually results in a coarse weld microstructure, a wide HAZ and lithium depletion in the weld zone, which can lead to low strength welds as well as low resistance to stress corrosion cracking. Common defects like hot cracking raise the need for dissimilar crack resisting filler materials (Madhusudhan Reddy and Gokhale, 2014). Friction based welding processes have shown superior performance when welding conventionally difficult to weld aluminum alloys as summarized by Çam and Mistikoglu (2014). To seal the exit hole at the end of the SSUBT–FSW process only a small number of friction based welding processes are published.

Most keyhole closure processes have only been employed in keyholes left by FSW and not in through holes. Examples are active–passive filling friction stir repairing and self-refilling friction stir welding. Active–passive filling friction stir repairing was introduced by Ji et al. (2016) and is a multi-stage process with different filler bits and pinless tools. In 2012 Zhou et al. (2012) introduced the self-refilling friction stir welding process. Self-refilling friction stir welding uses a series of non-consumable tools with gradual changes in pin geometry and size to self–refill a keyhole without filler material, which results in thickness reduction of the workpiece.

The only processes that have been employed to seal through holes in metallic workpieces are friction plug welding and refill friction stir spot welding. In friction plug welding (or friction taper plug welding) a tapered keyhole is sealed by a plug, with a taper similar to the hole, by forcing the rotating plug into the keyhole co-axially as employed by Du et al. (2016). In friction plug welding, the geometry of the plug has to be adapted to the tapered hole dimensions and machining is necessary on both sides of the workpiece to remove the not consumed parts of the plug from the top as well as the material that is extruded out of the plate from the bottom. Filling friction stir welding, presented by Huang et al. (2011), is derived from friction plug welding and adds a shoulder part to the tapered plug to avoid stress concentration at the interface between plug and hole. However, filling friction stir welding has only been used to seal keyholes left by FSW and not in through holes.

Reimann et al. (2016) introduced the refill friction stir spot welding (RFSSW) method (also known as friction spot welding, FSpW) to seal through holes in metals to solve problems such as damage to holes, broken tools or keyholes left at the end of FSW processes. Employing a plug made of the same material keyholes were sealed by joining the plug to the surrounding workpiece in AA 6061–T6 using the RFSSW process.

This method shows advantages including defect free welds, superior surface appearance on both sides of the weld and a high reproducibility that is not always achieved by competing processes. Additionally, this method does not need any surface preparation prior to or after the welding process and seals the keyhole in a single welding step.

To perform a keyhole closure weld, RFSSW uses a non-consumable tool consisting of three independent movable parts including a stationary clamping ring and two rotating parts—the sleeve and the probe. The RFSSW process starts with moving the clamping ring downwards to clamp the workpiece. The sleeve and probe start to rotate in the same direction at a preset speed. The sleeve plunges downwards into the workpiece while the probe is simultaneously retracted. The rotating sleeve generates frictional heat, plasticizing the workpiece material, and the downward movement of the sleeve forces the softened material into the cavity left by the probe. The sleeve diameter is larger than the diameter of the plug, which has previously been inserted into the keyhole. Thus, the interface between the plug and surrounding workpiece is completely stirred by the sleeve. When a predetermined plunge depth is reached, the rotating probe and the sleeve interchange their direction of movement. The sleeve moves upwards towards the initial position and the probe downwards, pushing the material back into the joint to refill the hole left by the retracting sleeve. Metallic bonding is created at the interface between the refilling plasticized material and the surrounding workpiece. Finally, the tool is retracted from the surface to leave the initial plug and surrounding workpiece completely joined.

In addition to the keyhole closure application, the RFSSW process is well known to produce solid-state welds in an overlap joint configuration in a wide range of lightweight alloys. In this conventional application, RFSSW has been successfully used to weld Al-Li alloys. Gao et al. (2015a) applied the RFSSW process to the aluminum–lithium alloy 2A97 and achieved sound joints. Pieta et al. (2014) investigated the RFSSW process parameters when joining AA 2198–T8 sheets, confirming the weldability of AA 2198 using RFSSW. The application of RFSSW as a method to refill keyholes has only been reported by Reimann et al. (2016).

In the current work, we addressed the above mentioned challenge to seal the exit hole at the end of the BT-FSW process and repair flaws in BT-FSW welds. Semi–stationary shoulder bobbin tool FSW (SS_UBT-FSW) was first employed to produce defect free welds with superior surface finish and mechanical properties in AA 2198–T851. In a second step, through holes in the center of the SS_UBT-FSW, welds were sealed using

the RFSSW process without any preparation work before welding as proposed by Reimann et al. (2016). As an attempt for classification, keyhole closure welds using RFSSW in SS_UBT-FSW welds and unwelded base metal were compared with SS_UBT-FSW butt welds.

2 Materials and Methods

2.1 Aluminum alloy 2198–T851

The aluminum-lithium alloy 2198 is a representative of the third generation of aluminum-lithium alloys and is applied as the sheet material. The temper used was T851 (solution heat treated, cold worked by 5% and artificially aged). The chemical composition is listed in Table 1 as taken from the AMS standard (Association, 2015). The alloy features a density of 2.69 g/cc and an E-modulus of 75 GPa.

Table 1: Chemical composition of alloy AA2198

Cu	Li	Zn	Mg	Mn	Zr	Fe	Al
3.2	1.0	0.014	0.31	0.005	0.076	0.046	Rem.

2.2 Experimental procedure

The base material was machined to produce samples measuring 400×75×3 mm which were subsequently butt welded perpendicular to the rolling direction using the SS_UBT-FSW process as shown in

Figure 1 a). The welded specimens were then cut into 35 mm segments perpendicular to the weld direction; see Figure 2. To apply the keyhole closure process, through holes of 7.5 mm in diameter were drilled in the center of the welded segments; see

Figure 1 b). Cylindrical plugs of the same material and identical diameter were produced by electric discharge machining. In the next step, the plug was fitted manually into the hole. Finally, RFSSW was used to join the plug and the surrounding workpiece eight days after the initial butt welding; see

Figure 1 c). This creates an RFSSW keyhole closure weld in the center of the SS_UBT-FSW butt welded structure; see Figure 1 d). Details of the RFSSW keyhole closure process can be found in (Reimann et al., 2016).

To characterize the keyhole closure process in SS_UBT-FSW welds, three batches of samples were produced: SS_UBT-FSW welds, RFSSW keyhole closure welds and RFSSW keyhole closure welds in the

SS_UBT-FSW weld seam as described above. For mechanical testing, eight samples of each batch were produced with one set of process parameters each. For thermal cycle measurements, two samples were welded according to the sample geometry in Figure 2. The base metal properties were averaged over three samples.

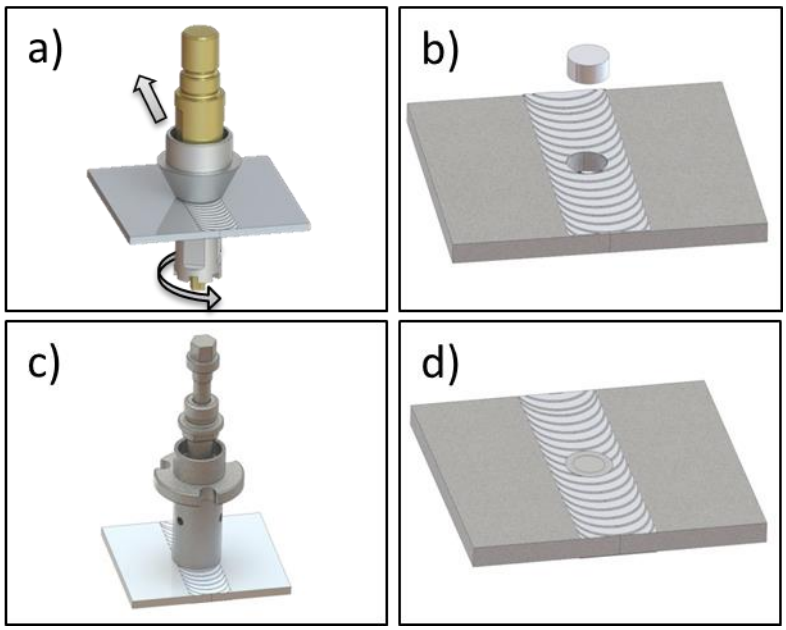

Figure 1 Process chain of SS_UBT-FSW termination hole closure using RFSSW: a) SS_UBT-FSW process, b) keyhole simulating termination hole, c) RFSSW process, d) closed keyhole and final weld seam.

2.3 Welding processes

The SS_UBT-FSW welds were produced using a modified five-axis parallel-kinematic robot system (PKM T805) equipped with a specially designed BT-FSW weld head capable of operating in self-reacting or gap controlled mode. The BT-FSW weld head can produce welds with both rotating shoulders (BT-FSW), both stationary shoulders (SSBT–FSW) as well as with upper-stationary (SS_UBT-FSW) or a lower-stationary shoulder (SS_LBT-FSW). The tools were dimensioned to a 7 mm diameter, featured probe and two 15 mm diameter shoulders. The lower shoulder is attached to the probe and rotates with the same speed while the upper shoulder was held stationery by a decoupling system. The probe was made of the nickel–cobalt alloy MP159, whereas the shoulder material was molybdenum–vanadium hot work tool steel (X38CrMoV5-1).

The welding parameters were adjusted to a rotational speed of 400 rpm and a transverse speed of 500 mm/min. The process was run in self-reacting mode at 5000 N, allowing the gap width to vary. Further details of the process can be found in the work of Goebel et al. (2016).

The RFSSW welds were produced with custom-built equipment designed and constructed to investigate this process. The axial and rotational movement of the tool parts is actuated by individual electromechanical transducers. Plunge depth and rotational and axial speed were controlled using value response from the position control system in the drive amplifier in 10 ms steps. The axial load of the probe and sleeve are measured using four identical load cells each, whereas the axial load of the clamping ring was measured using three load cells. The torque of the sleeve and probe were measured using load sensors attached to the respective motors via lever arms. The motors were float-mounted, so the engine torque was transferred to the load cells. The used load cells were customized to the respective measurement range and had a sensor inaccuracy of 0.8 %. The measurements were coupled with a data acquisition system so that the force, torque and position values were recorded simultaneously during each spot welding operation. To display the sleeve and probe torque in Figure 5, a moving average of 3 measurement values was calculated.

The keyhole closure welds were carried out according to the sleeve plunge process reported by Reimann et al. (2016). The spot welding equipment produced the welds in position control mode. The clamping ring moves to a predefined position on the surface of the workpiece, and the welding operation is carried out by monitoring and controlling the positions of the individual tool parts.

Threaded RFSSW tools made of molybdenum–vanadium alloyed hot work tool steel with a 17 mm diameter clamping ring, a 9 mm sleeve and a 6 mm probe were utilized. The welding parameters in this study were a rotational speed of 1000 rpm and plunging or retracting speed of the sleeve of 0.85 mm/s. Dwell time was not used. The plunge depth of the sleeve was set to 2.90 mm, which is 96.7% of the sheet thickness. The used process parameters are optimized to produce defect free keyhole closures in AA 2198–T851.

2.4 Analysis and testing techniques

The keyhole closure RFSSW process is analyzed by evaluation of the behavior of characteristic process variables. Thermal cycle analysis was performed to understand the exposure of the base metal to process

heat during keyhole closure welds. SS_UBT-FSW, RFSSW and SS_UBT-FSW + RFSSW welds were compared by microstructural features and local and global mechanical performance.

The thermal cycle was recorded in the heat-affected zone (HAZ) during the RFSSW operation, 4 K–type thermocouples were embedded in the aluminum sheets at a depth of 1.5 mm from the surface of the sheet and 9 mm and 17 mm from the center of the weld; see Figure 2. The final results at the two distances are then averaged from two measurements each.

For the microstructural analysis, samples were sectioned perpendicular to the welding direction and prepared by standard metallographic specimen preparation procedures using flat grinding and finish polishing. For microstructural analysis using polarized light microscopy, samples were anodized using a 3 vol pct solution of HBF4 known as BARKER solution at 22 V for 2 min. The grain size was measured employing a LEICA software following the ASTM E112-13 standard.

Mechanical testing was performed on three batches: the SS_UBT-FSW welds, the RFSSW welds and the combined processes. The testing dimensions of all coupons were kept constant and left at room temperature for four weeks, allowing natural aging to take place and have a stable microstructural condition. Samples were machined to a dog-bone shape tailored for spot weld testing with a gauge length of 50 mm and a width of 13.5 mm; see Figure 2. Tensile tests were carried out in accordance with ISO 6892-1:2009 testing perpendicular to the rolling direction with a speed of 1 mm/min. The hardness measurements were conducted on a Zwick Vickers hardness tester (LECO, type M-400-H) in accordance with ISO 6507-1:2005 (applying 0.2 kg for 10 s).

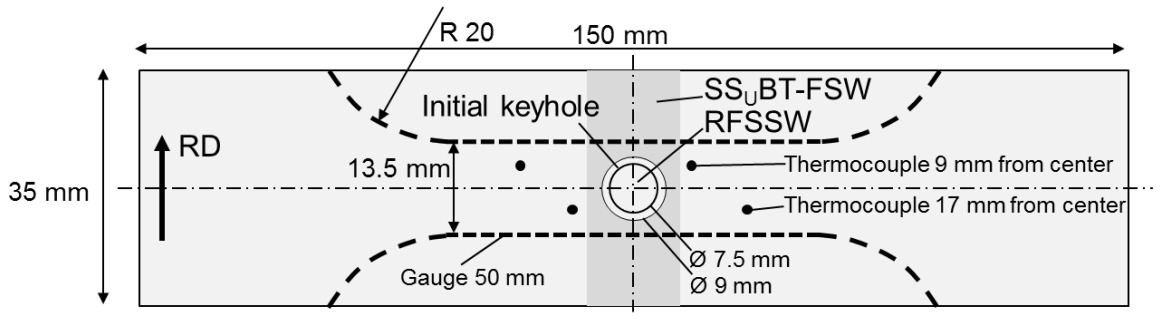

Figure 2 **RFSSW welded coupons**

2.4.1 Correction method for measurement of circular features in spot welds

When cross-sectioning an RFSSW spot, it is particularly important to section the sample in the exact middle of the spot weld to ensure dimensional correctness between different cross sections. Standard metallographic preparation procedures do not deliver the needed accuracy. To overcome the problem of inaccurate microstructural measurements due to the position of the cross section, a correction method has been introduced, which applies to measurements of circular microstructural features – for example the weld zones.

The gap between the sleeve and clamping ring of the RFSSW tool leaves a circle of protruding material on the surface of the sheet. In a cross section, the distance between the protruding material should be equal to the outer sleeve diameter when cross-sectioning the samples in the exact center of the spot weld. The distance a of the cross section to the ideal cross section through the center of the weld is calculated using the distance between the protruding parts l_p and the sleeve diameter d_s; see Figure 3:

$$a = \sqrt{\left(\frac{d_s}{2}\right)^2 - \left(\frac{l_p}{2}\right)^2} \tag{1}$$

Assuming that the macrostructural features are circular in an RFSSW, the measured width of a circular feature x_1 to x_2 will be smaller than the true radial width w; see Figure 3. The true distance of point x_1 to the center of the weld is calculated using the measured distance of the point to the center of the weld in the used cross section:

$$x_{1_{real}} = \sqrt{x_{1_{measured}}^2 + a^2} \tag{2}$$

The true distance of point x_2 to the center of the weld can be calculated analogously. Finally, the true width of the circular feature can be calculated as

$$w = x_{2_{real}} - x_{1_{real}} \tag{3}$$

The above-mentioned correction method applies to horizontal measurements of distance in or of circular features only. In RFSSW, it applies to measurements of the width of weld zones, for example, but not to the measurement of grain sizes.

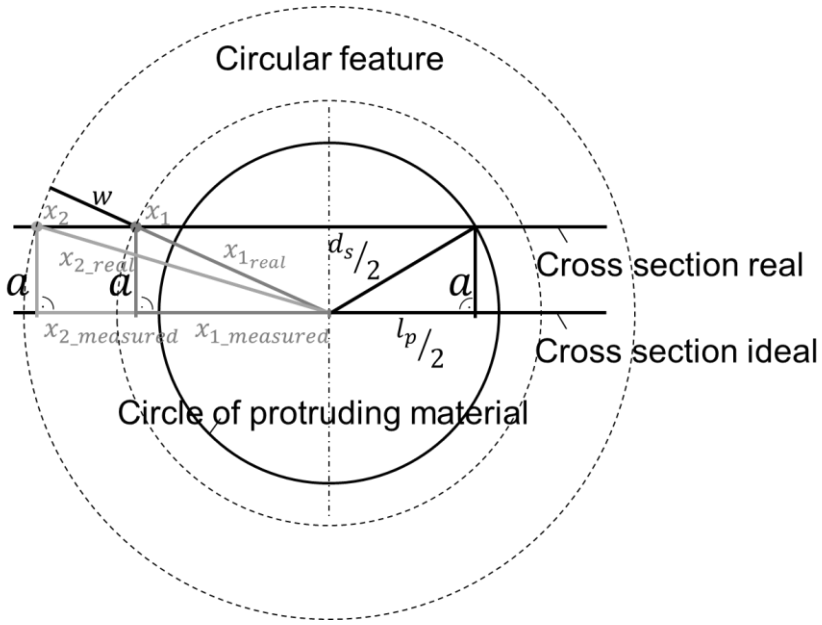

Figure 3 **Measurement of circular features in cross sections**

3 Results & Discussion

3.1 Keyhole closure process

The RFSSW keyhole closure weld shows the characteristic behavior of the tool position and rotational speed over process time; see Figure 4. In the diagram, the surface of the welded sheet is defined as tool position 0; positive values of the tool position describe the direction downwards into the workpiece.

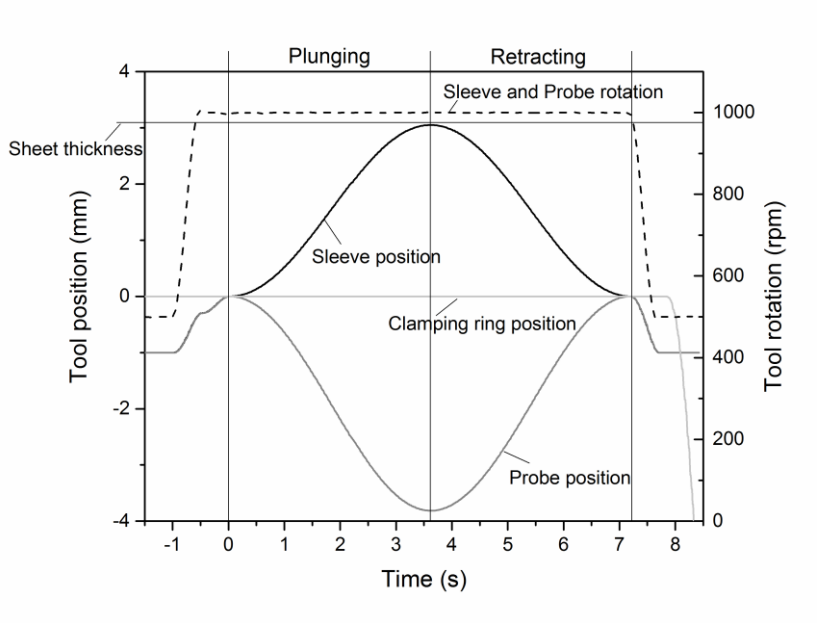

Figure 4 **Measurement of positions and rotational speed during RFSSW keyhole closure welding**

The clamping ring moves to the initial position on the surface of the sheet, holding this position for the rest of the welding process; see Figure 4. The sleeve and probe are retracted 1 mm from the surface of the sheet to prevent friction generation before the process starts. In a first step, the rotation of the sleeve and probe are accelerated to 1000 rpm, and they are moved downwards to 0.3 mm above the sheet surface. Immediately after that, the moving tool parts plunge downwards to touch the surface of the sheet while maintaining a constant rotational speed. The actual welding process starts with the sleeve being plunged into the workspace while the probe is retracted. To constrain the plasticized material that has been displaced by the sleeve into the cavity left by the retracting probe, the probe is retracted further than the sleeve plunges downwards owing to the different front surface sizes of the sleeve and probe. Thus, the axial speed of the retracting probe is higher than the 0.85 mm/s plunging speed of the sleeve. The rotational speed of the

moving parts is identical during the welding process. Therefore, the only remaining relative movement between probe and sleeve is the axial movement. The RFSSW keyhole closure process ends with the clamping ring being lifted from the surface of the sheet.

A typical distribution of tool forces and torque is shown in Figure 5. The positive forces describe force downwards in the direction of the plunging tool.

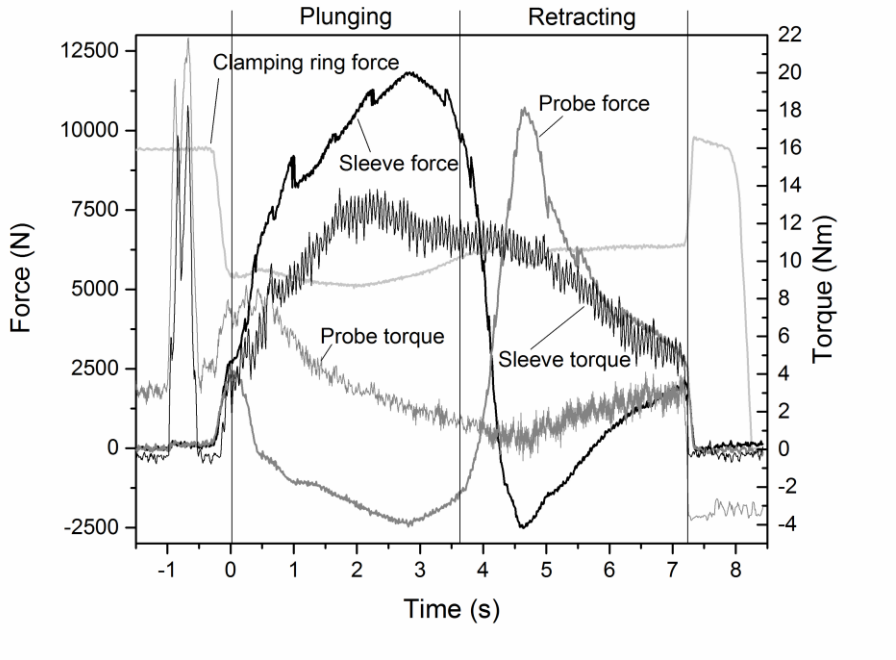

Figure 5 **Force and torque during RFSSW keyhole closure**

The clamping force needed to move the clamping ring to the initial position of the welding operation is 9 kN. The clamping force is reduced when the rotating tool parts move downwards to the surface of the sheet, transferring axial forces. During the welding operation, the clamping force stays at a lower level of approximately 6 kN. With initial contact to the sheet, the sleeve force increases while the probe force decreases in the first half of the process. The highest force on the sleeve of 11.8 kN is reached after 3 s during the plunging of the sleeve immediately before the axial speed of the sleeve is reduced, compared to the sleeve position shown in Figure 4. From the highest value the sleeve force decreases to below zero to accelerate the sleeve and associated movable parts in the reverse direction. The probe force behaves opposite to the sleeve force. The minimum of approximately minus 2500 kN is reached when the sleeve maximum appears, and the force increases afterward to a maximum of 10.7 kN during the sleeve-retracting

phase of the process, indicating that in this phase, the material is pushed down by the movement of the probe. With the tool parts approaching the upper surface of the sheet in the end phase of the process, both probe and sleeve force approach low values of a force of 1–3 kN.

The sleeve and probe torque show a significant increase approximately 1 s before the process starts. This increase is needed to accelerate the tool parts to the set rotational speed. The sleeve and probe torque start at similar values of approximately 6 Nm at the beginning of the process when both tool parts are touching the surface of the aluminum sheet. During the plunging phase, the sleeve torque increases to approximately 11 Nm, remains at a high level until the set plunge depth is reached and decreases back to the initial values during the retraction phase. The sleeve torque is related to the plunge depth (Figure 4) indicating correlation with the surface area of the rotating sleeve being in contact with the surrounding workpiece, creating frictional resistance. The slight decrease in sleeve torque values is assumed to be caused by the softening of the base material in contact with the sleeve. The probe torque decreases during the first half of the process. With no relative rotational motion between probe and sleeve, this is assumed to be related to the softening of the base material in contact with the probe. The probe torque increases with the downward movement, causing the plasticized material to be forced against the front surface of the probe, generating frictional resistance.

At the end of the process, the tool parts move upwards, and the clamping force increases back to the initial values of 9 kN to hold the position because the other tool parts no longer transfer any force.

To calculate the total energy delivered during RFSSW keyhole closure, an approach similar to that introduced by Su et al. (2006) for friction stir spot welding (FSSW) is applied. The energy is determined by axial force, penetration depth, rotational speed and torque according to

$$Q_{applied} = \sum_{n=1}^{n=N} Force(n)(x_n - x_{n-1}) + \sum_{n=1}^{n=N} Torque(n)\omega(n)\Delta t \quad (4)$$

where x_n is the penetration depth at sample (n), ω is the angular velocity (rad s^{-1}), n is the sample number, N is the final sample, and Δt is the sampling time.

The equation must be applied to the probe and sleeve measurements. The energy generated during the spot welding is calculated as 7.36 kJ. Similar to the findings of Su et al. (2006) for FSSW, the contribution resulting from tool rotation is 160 times higher than that due to tool penetration. The SS_UBT-FSW process in identical material conducted by Goebel et al. (2016) showed an energy input per unit length of 219 J/mm. For a 35 mm weld length (equal to the used sample width; compare with Figure 2), this equals 7.67 kJ being delivered in the same sheet dimension used in this study.

The energy used for weld zone formation and the energy dissipated in the aluminum sheet can be different in both welding processes because of different welding equipment, tool dimensions and general heat transfer conditions. Additionally, different sample geometries impede the comparability of temperature distribution in the aluminum sheets.

3.2 Thermal cycle analysis

Thermal cycle measurements were conducted 9 mm and 17 mm from the center of the weld. The thermal cycle shows a typical behavior in the heat-affected zone during RFSSW. The temperature rises during the plunging phase of the sleeve with 75°C/s and 34°C/s at the measured positions, respectively. During the second half of the process, from the beginning of sleeve retraction to the highest temperatures at the measured positions, the heating rate is significantly lower with 14°C/s and 19°C/s. Nine millimeters from the center of the weld the peak temperature of 333°C is reached at 6 s after the beginning of the process and during the retraction of the sleeve. Seventeen millimeters from the center of the weld, the highest temperature of 227°C is reached after the withdrawal of the tool. After approximately 15 s after the beginning of the process, the temperature in the tested coupon seems to be homogeneous at approximately 170°C in both measurement locations.

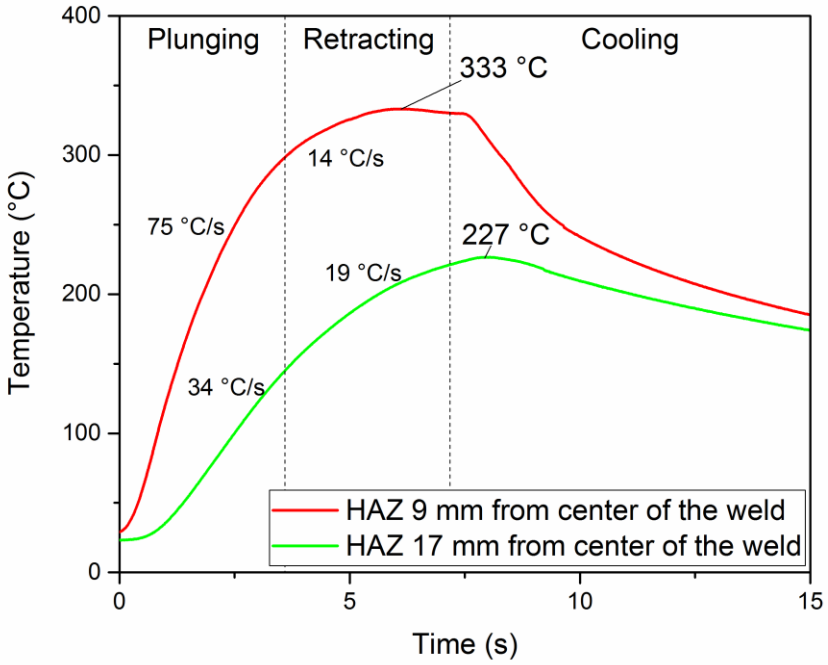

Figure 6 Thermal cycle of keyhole closure welds using RFSSW

Compared with the thermal cycle during SS_UBT-FSW welds recorded and discussed by Goebel et al. (2016), the thermal cycles at similar distances from the weld center are similar. Regarding the peak temperatures reached approximately 9 mm from the center of the weld, no difference between the welding processes

could be measured, whereas a difference can be observed in terms of temperature exposure. The RFSSW keyhole closure process exposes the surrounding base material to higher temperatures for a longer period of time. Temperatures above 150°C were measured for 20.15 s and above 300°C for 4.6 s. The exposure times of the SS$_U$BT-FSW process were measured to 17.98 s and 3.66 s, respectively. As the calculated energy input is similar in 35 mm wide samples, different thermal cycles are mainly caused by changing energy input location in linear friction welding compared to stationary RFSSW as well as different sample dimensions and general heat transfer conditions.

3.3 Microstructural features

Figure 7 a) presents the cross section of a RFSSW keyhole closure weld. The macrograph displays a defect free microstructure where no lack of refill or voids can be observed. The microstructure of the plug and the interface between the initial plug and surrounding workpiece is not visible in the shown cross-section (Figure 7 a) since it is completely stirred and recrystallized. Two features of protruding material on the surface of the sheet can be observed and used to calculate l_p; see chapter 2.4.1. The RFSSW microstructure features three typical zones consisting of a stirred zone (SZ), which is surrounded by a thermo-mechanically affected zone (TMAZ) and a heat-affected zone (HAZ). The SZ experienced the highest shear rates and temperatures and consists of fully recrystallized, equiaxed grains with an averaged grain size of 6.13 µm. The SZ is wider than the sleeve diameter and curved convex to the surrounding zones. Applying the correction method introduced in chapter 2.4, the size of the SZ has been measured. At mid-thickness, the SZ is 920 µm wider than the sleeve diameter, indicating high shear rates and temperatures leading to dynamic recrystallization on the outside of the rotating sleeve. The TMAZ experiences moderate temperatures and strain rates leading to upward-bended grains in the direction of the retracting direction of the sleeve. The TMAZ has a torus-like shape that is concavely arched away from the stirred zone. In the upper parts of the spot weld, the TMAZ shows the broadest extension and is tapered to the upper and lower surfaces of the sheet. The HAZ is affected only by the thermal cycle and experiences no plastic deformation. The grain size corresponds to the grains of the unaffected base material with pancake-shaped grains resulting from the rolling process measured at 11 × 4 µm. Overall, the microstructural features correspond to typical characteristics of RFSSW, as shown, for example, by Amancio-Filho et al. (2011) in AA 2024. The keyhole closure welds show the same flawless appearance with high surface quality as those reported in AA 6061–T6 (Reimann et al., 2016).

The cross section macrograph of the SS$_U$BT-FSW weld is presented in Figure 7 b). No defects were observed. The SS$_U$BT-FSW weld features an asymmetrical shape widening up towards the rotating, lower shoulder. Similar to the conventional BT–FSW macrograph shown by Wang et al. (2015), the hourglass shape resulting from the presence of two shoulders is visible. Similar to RFSSW, the macrostructure reveals typical welding zones consisting of a centered SZ connected by the TMAZ and the HAZ to the base material. 1.5 mm millimeters from the sheet surface, the SZ is 8.03 mm wide and consists of fully recrystallized,

equiaxed grains with an average size of 5.66 µm. The SZ is widened to the RS owing to extrusion of hot, sheared material around the probe as reported by Colligan (1999). The grains in the TMAZ deform along the vertical direction. Analogous to the RFSSW weld, the HAZ shows no changes in microstructural features compared with the BM.

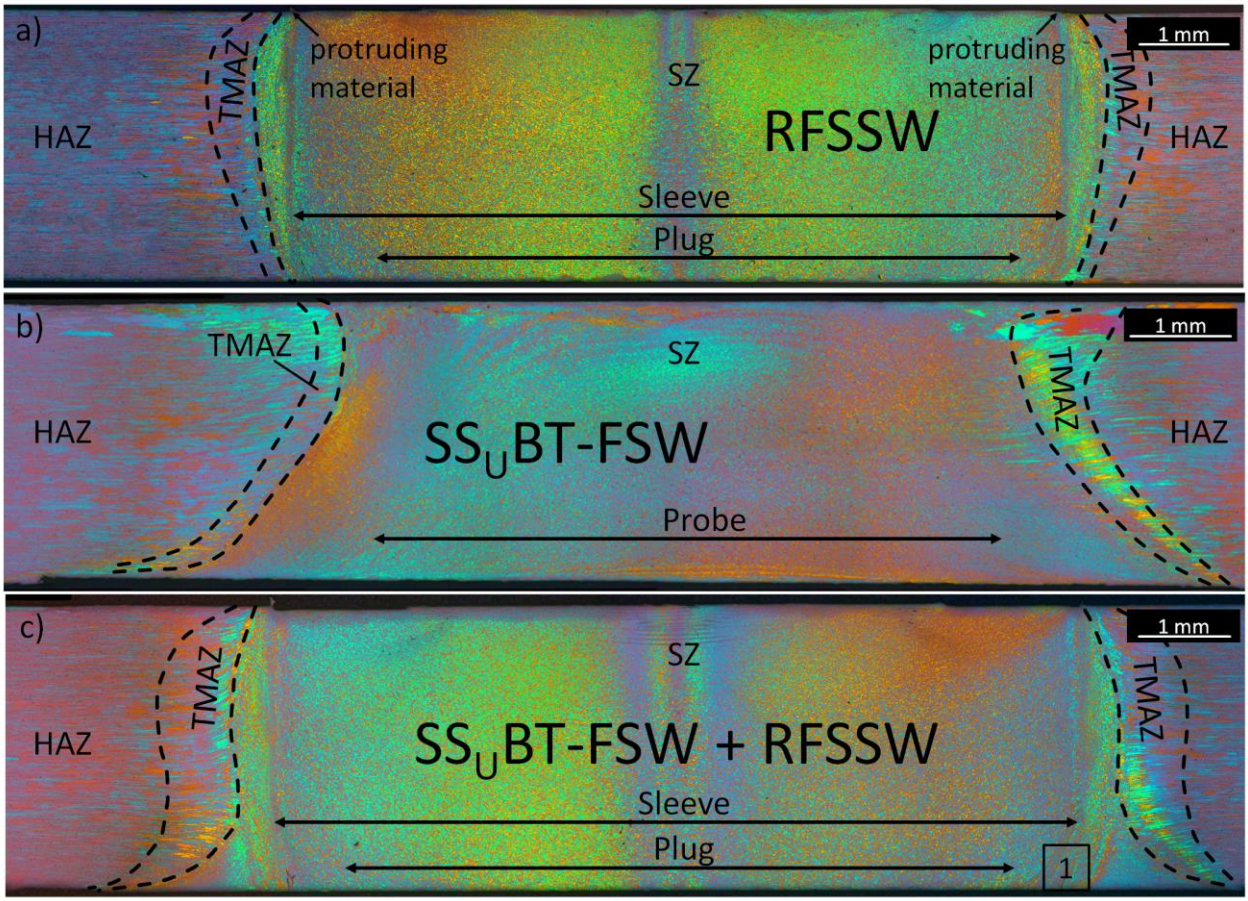

Figure 7 Low magnification Barker-etched overview of welded samples: a) keyhole closure weld using RFSSW, b) butt joint using SSUBT-FSW c) keyhole closure weld using RFSSW in SSUBT-FSW weld seam

In Figure 7 c), the macrostructure of the combined processes is shown. It can be observed that RFSSW is the governing process because the weld zones developed similarly to the weld zone formation of the RFSSW process (Figure 7 a)). This was expected because the RFSSW tools are larger in diameter, and the process was run after the SSUBT-FSW process. Still, characteristic remnants of the SSUBT-FSW process are still visible. The weld zone distribution is similar to the observations in RFSSW; additionally, a broadened TMAZ and the shoulder-induced SZ on the lower side remaining from the SSUBT-FSW process can be observed. The size of the SZ is similar to the single RFSSW process. Otherwise no significant differences could be measured.

The mid-thickness broadening of the TMAZ, which increased by a magnitude of approximately 1.5 compared to the single RFSSW process, shows a higher deformation and longer thermal influence where prior HAZ material is transformed into grains more coarsened and deformed. The grain size in the SZ was measured to 5.7 µm, only slightly different from the grain sizes measured in the single processes. The grains in the SZ in the lower, outer corners (remaining SZ from the SSUBT-FSW process) are affected by the thermal cycle of the RFSSW process only and experience no further deformation; therefore, the grain size is slightly increased.

At higher magnification, the irregularities in the region of the outer sleeve are found as remnants from the interface between the plug and surrounding workpiece, assumed to be accumulated oxides; see Detail 1 of Figure 7 c) in Figure 8. A similar phenomenon has been reported when butt joining aluminum workpieces using friction stir welding by Sato et al. (2004). The joint line remnants was found to be fine dispersed Al_2O_3 particles that did not affect the root-bend property of the weld. For keyhole closure using RFSSW this phenomenon is currently under investigation. It should be noted that the position of these remnants differs from the initial position of the interface between the plug and surrounding workpiece, the remnants are deployed further from the center of the weld during the refilling stage of the process. The remnants are assumed to be caused by insufficient stirring during the welding process in the areas underneath the rotating sleeve and can be avoided by employing a higher plunge depth.

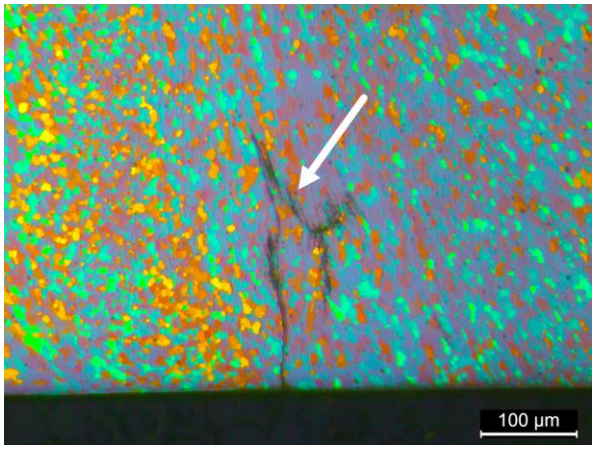

Figure 8 **Remnant from the interface of plug and surrounding workpiece at lower parts of RFSSW weld spot**

3.4 Mechanical properties

3.4.1 Microhardness

The microhardness distribution along the centerline on the cross-section of all three processes is presented in Figure 9. All processes develop a W-shape hardness distribution, which was often reported for high-strength, precipitation-hardened aluminum alloys welded in artificially aged condition—e.g., by Shen et al. (2013) for RFSSW in AA 7075–T6. or for conventional friction stir welding in AA 7075–T6 by (İpekoğlu et al., 2013a), in AA 6061–T6 by İpekoğlu et al. (2013b) and in AA 6063–T5 by Sato et al. (1999). Additionally, a similar hardness distribution was found by Pieta et al. (2014) in Al-Li alloy 2198–T8 refill friction stir spot welded sheets.

It is assumed that the variation of microhardness in different regions of FSW joints is associated with the evolution of the metallurgical state in precipitate-hardened aluminum alloys (Gao et al., 2015b). Zhang et al. (2014) studied the ageing response of AA 2198. They found that the precipitation sequence of the aluminum-lithium alloy 2198 results in a complex microstructure that holds several precipitates finely dispersed. The greatest contribution to the overall strength is during artificial aging forming T1 (Al_2CuLi) and the during natural aging formed δ′ (AL3Li). The amount of T1 is highest in the peak aged temper (T8), so the BM exhibits the highest hardness of 149 $HV_{0.2}$.

The hardness distribution of the processes analyzed is not significantly different. The stirred zones show a relatively constant hardness of 110 $HV_{0.2.}$ With the beginning of the TMAZ, the hardness decreases continuously to a minimum of approximately 100 $HV_{0.2}$ in the HAZ. From there, the hardness increases to base metal values with decreasing exposure to higher temperatures, compared to the thermal cycles shown in Figure 6. At the end of the HAZ, the base metal values are reached approximately 15 mm from the center of the weld.

In the SZ and adjacent areas, the material is believed to be exposed to temperatures above the solubilization temperatures of the precipitates (Goebel et al., 2016). This would lead to partial or complete supersaturated matrix prone to natural aging processes after welding. In the natural aging process, the hardening precipitate δ′ is formed and contributes to the SZ hardness of 110 $HV_{0.2}$. The dynamically recrystallized grains in the SZ might contribute due to grain–boundary strengthening following the Hall-Patch effect to higher hardness.

The point of lowest hardness is an important characteristic for every weld because the strain concentration will occur and lead to failure in this region. Its location depends on the tool dimensions and the heat input. The point of lowest hardness in SS_UBT-FSW is located 5 mm from the weld center, whereas in RFSSW and the combined process, it is at 7 mm. With increasing heat input, the artificially aged T1 phase becomes dissolved, whereas the high temperatures and stirring lead to a supersaturated aluminum matrix prone for natural aging processes, similar to the findings of De Geuser et al. (2014) in AA 2050. The region of lowest hardness is located at the point where the process thermal cycle is the most unfavorable influencing these two mechanisms. The longer exposure to higher temperatures explains that the areas of lowest hardness are further from the center of the weld in RFSSW.

The thermal cycle 17 mm from the weld center reported in section 3.2 does not affect the BM mechanical properties. No changes in hardness can be observed at this distance from the center of the weld. Nine millimeters from the center of the weld, the hardness is significantly reduced, Figure 9. The thermal cycle at this position significantly changes the existing precipitation structure. At this position, neither microstructural changes nor changes in grain size or form were observed as reported in section 3.3. De Geuser et al. (2014) performed a series of heat treatments mimicking the temperature exploration during the FSW process in a 2050 Al-Li-Cu alloy. Their findings indicate that short intervals at temperatures below 250°C should not modify the precipitate morphology. This is consistent with the finding that the temperature cycle 17 mm from the weld center does not affect the hardness in this region.

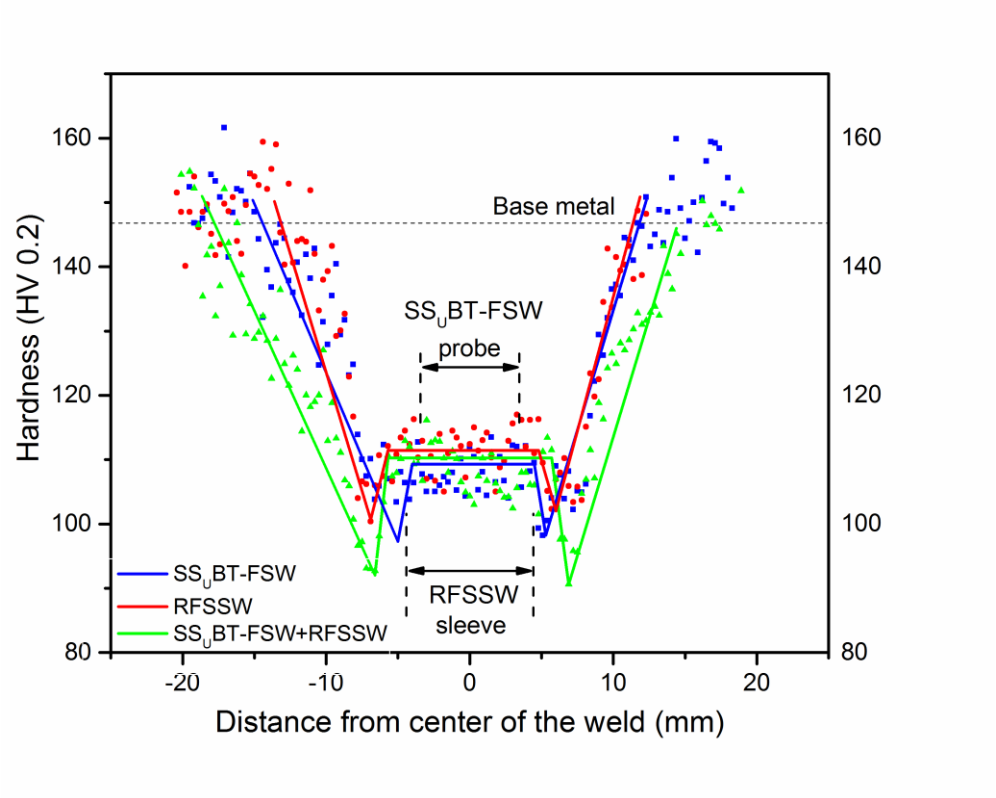

Figure 9 **Microhardness measurements of single SS_UBT–FSW and RFSSW as well as combined processes**

3.4.2 Analysis of tensile characteristics

For the evaluation of the mechanical behavior under monotonic uniaxial loading, tensile tests were conducted. All processes were tested as-welded with no further surface or heat treatment. An overview of representative stress–strain curves and statistical data are given in Figure 10. The base metal results confirm the literature data in the LT direction. The SS_UBT-FSW weld fractured at the highest values, showing 412 MPa ultimate tensile strength (UTS) and 274 MPa yield strength (YS), which correspond to 80 % and 59 % of the BM values, respectively. The coupons of the RFSSW process and the combined processes performed similarly, resulting in a UTS of 78 % and YS of 57 % of the BM strength. The longer exposure to higher temperatures explains the lower yield strength and ultimate tensile strength of RFSSW samples.

As known from friction welded precipitation-hardened aluminum alloys tested under tensile loading, yielding first occurs in the region of lowest hardness (Figure 9). Almost complete strain will accumulate in this region,

resulting in lower elongation compared with BM. Between the friction processes, the results show the tendency to higher elongation values for the SS_UBT-FSW process.

In summary, the thermal cycle of the RFSSW process weakens the surrounding microstructure more strongly than the SS_UBT-FSW process, see section 3.2. When performing an exit hole closure or flaw repair using RFSSW, the workpiece material is first exposed to the SS_UBT-FSW thermal cycle and then to the RFSSW thermal cycle. The tensile strength characteristic of the combined processes is similar to the single RFSSW welds. This indicates that the softening impact of the combined processes on the BM is governed by the RFSSW thermal cycle. The thermally modified material left by the SS_UBT-FSW seems to react similarly to the BM when exposed to the RFSSW thermal cycle.

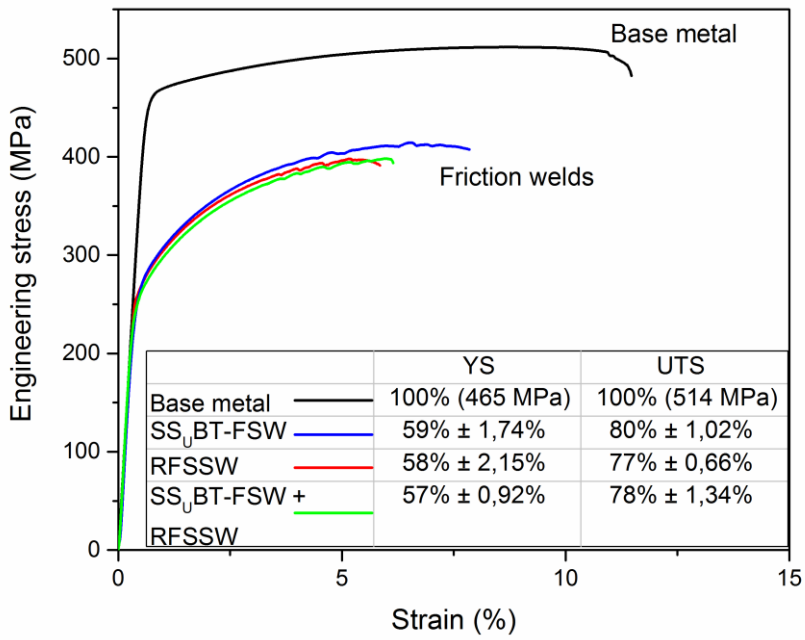

Figure 10 Tensile characteristic of single SS_UBT–FSW and RFSSW as well as combined processes

After testing, the samples were characterized with regard to failure modes. Two modes could be identified throughout all coupons: failure mode 1 fractured in the HAZ in the region of the lowest hardness, whereas mode 2 fractured in the SZ. The single SS_UBT-FSW and RFSSW process welds failed, showing failure mode

1 as shown in Figure 11. Combining the processes, failure mode 1 and failure in the outer regions of the SZ (failure mode 2) occurred.

The two identified failure modes suggest two main weakened areas in the welded samples. The first one is the metallurgical notch introduced by the thermal cycle that can be observed in the hardness distribution and will result in a fracture in the HAZ. The second one is the outer region of the SZ with the interface remnant as shown in Figure 8, the welded interface created by the refilled material being distributed against the surrounding material by the downwards movement of the probe in the second phase of the RFSSW process and the transition zone from SZ to TMAZ with grain size gradients. Failure in this region will result in a fracture in the SZ (mode 2). This mode 2 failure has been observed by the authors in different high strength aluminum alloys when employing RFSSW as keyhole closure technique. It is assumed to be caused by crack initiation in the interface remnant and crack propagation through the external areas of the SZ.

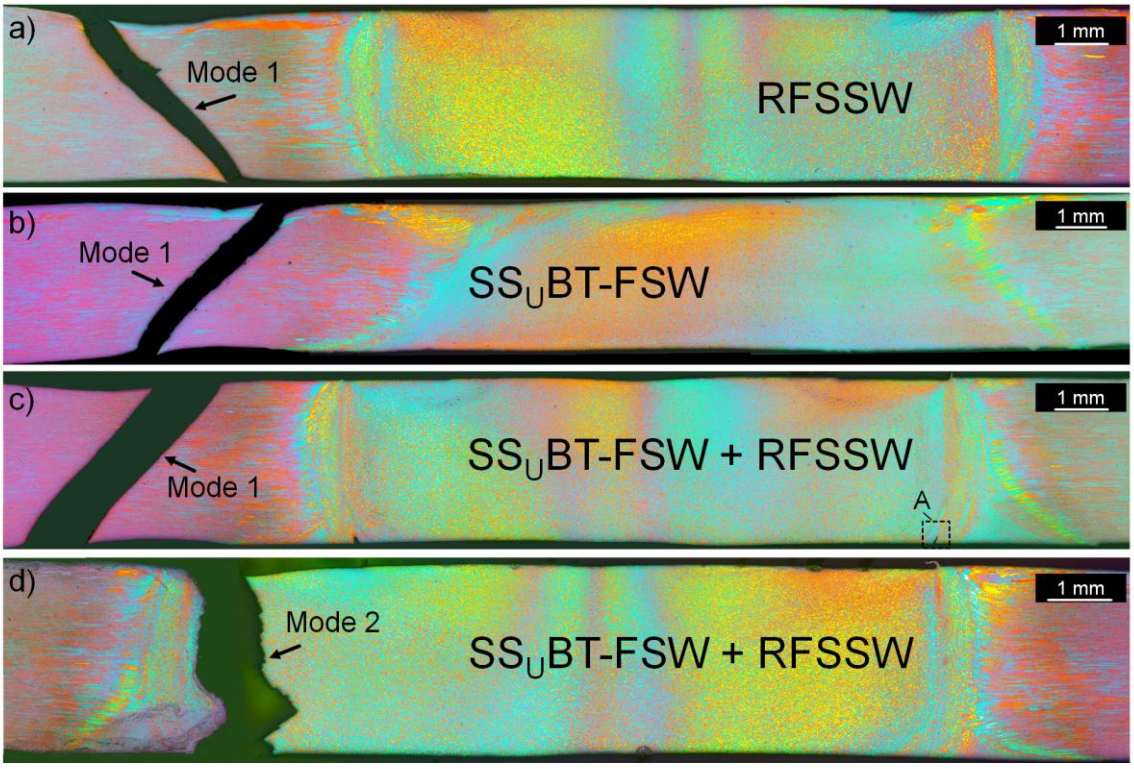

Figure 11 Failure modes in tensile test: a) mode 1 failure in keyhole closure weld using RFSSW, b) mode 1 failure in butt joint using SS_UBT-FSW, c) mode 1 failure in keyhole closure weld using RFSSW in SS_UBT-FSW weld seam, d) mode 2 failure in keyhole closure weld using RFSSW in SS_UBT-FSW weld seam

Some RFSSW cross sections show cracks in the lower parts of the SZ; see detail A of Figure 11 in Figure 12. These microstructural openings are believed to be initiated from the oxide remnants of the interface between the plug and sourrounding workpiece observed in the microstructure analysis (Figure 8).

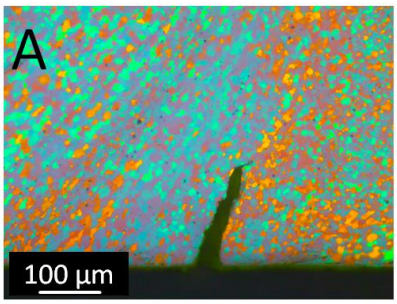

Figure 12 Crack initiation at the remnant from the interface between the plug and the surrounding workpiece

4 Conclusions

In this work, a solution for closing termination holes or flaw repairs using RFSSW is presented. Semi–stationary shoulder bobbin tool friction stir welding is employed to produce high-quality welds in AA2198–T8. Keyholes in SS_UBT-FSW were sealed using RFSSW. A systematic investigation comparing and combining the processes is given.

Conclusions:

1. RFSSW was presented as a keyhole closure technique for SSBT-FSSW welds and successfully applied for the first time to AA 2198–T851. The results show defect free and highly efficient joints. This study proves the ability of RFSSW to be applied as a termination hole closure technique.
2. The process parameter analysis of RFSSW keyhole closure revealed a high sleeve force of 12 kN during the plunging phase and a probe force of 11 kN during the retracting phase of the process. The processual torque is mainly applied by the sleeve with correlation to the plunge depth and maximal torque of 11 Nm. The energy input of RFSSW spot welds was calculated as 7.36 kJ.
3. The study revealed the thermal cycle during RFSSW keyhole closure welding with heating rates of 75°C/s and maximum temperatures of 333°C at 9 mm from the center of the spot weld. The exposure time to high temperatures is slightly longer in RFSSW keyhole closure welds compared with SS_UBT-FSW welds. When performing RFSSW keyhole closure welds in an SS_UBT-FSW weld seam, the higher thermal imprint of RFSSW drives the overall mechanical performance.
4. Microstructural analysis revealed flawless welds holding typical microstructural features for single SS_UBT-FSW and RFSSW welds. When the processes were combined to apply a keyhole closure technique, remnants of the SS_UBT-FSW SZ microstructure are observed surrounding the lower parts of RFSSW weld spots.
5. The mechanical performance of the closed holes using RFSSW in SS_UBT-FSW welds is similar to the performance of RFSSW keyhole closure welds in the base material. Efficiencies of 67 % in hardness, 57 % in YS and 78 % in UTS were achieved.

Acknowledgments

This work has been conducted within the framework of a technology transfer project (“REPSPOT - Keyhole closure using FSpW”) between Luthansa Technik AG and Helmholtz-Zentrum Geesthacht GmbH.

5 References

Amancio-Filho, S.T., Camillo, A.P.C., Bergmann, L., Santos, J.F.d., Kury, S.E., Machado, N.G.A., 2011. Preliminary Investigation of the Microstructure and Mechanical Behaviour of 2024 Aluminium Alloy Friction Spot Welds. Materials Transactions 52, 985-991.

Association, T.A., 2015. International Alloy Designations and Chemical Composition Limits for Wrought Aluminum and Wrought Aluminum Alloys. The Aluminum Association, Arlington, VA, USA.

Çam, G., Koçak, M., 1998. Progress in joining of advanced materials. International Materials Reviews 43, 1-44.

Çam, G., Mistikoglu, S., 2014. Recent Developments in Friction Stir Welding of Al-alloys. J Mater Eng Perform 23, 1936-1953.

Colligan, K., 1999. Material Flow Behaviour during Friction Stir Welding of Aluminum. Welding Journal 78, 229-237.

De Geuser, F., Malard, B., Deschamps, A., 2014. Microstructure mapping of a friction stir welded AA2050 Al–Li–Cu in the T8 state. Philosophical Magazine 94, 1451-1462.

Ding, R.J., Oelgoetz, A., 1996. Auto-adjustable pin tool for friction stir welding, US.

Du, B., Sun, Z., Yang, X., Cui, L., Song, J., Zhang, Z., 2016. Characteristics of friction plug welding to 10 mm thick AA2219-T87 sheet: Weld formation, microstructure and mechanical property. Materials Science and Engineering A 654, 21-29.

Gao, C., Gao, R., Ma, Y., 2015a. Microstructure and mechanical properties of friction spot welding aluminium–lithium 2A97 alloy. Materials & Design 83, 719-727.

Gao, C., Zhu, Z., Han, J., Li, H., 2015b. Correlation of microstructure and mechanical properties in friction stir welded 2198-T8 Al–Li alloy, Materials Science and Engineering: A, pp. 489-499.

Giummarra, C., Thomas, B., Rioja, R.J., 2007. New aluminum lithium alloys for aerospace applications, Proceedings of the light metals technology conference, pp. 19-20.

Goebel, J., Reimann, M., Norman, A., dos Santos, J., 2016. Semi-stationary shoulder bobbin tool friction stir welding of AA 2198-T851. Submitted for publication - Journal of Materials Processing Technology 11-25-2016 (PROTEC-D-16-02723) XX.

Huang, Y., Han, B., Tian, Y., Liu, H., Lv, S., Feng, J., Leng, J., Li, Y., 2011. New technique of filling friction stir welding. Science and Technology of Welding and Joining 16, 497-501.

İpekoğlu, G., Erim, S., Çam, G., 2013a. Effects of temper condition and post weld heat treatment on the microstructure and mechanical properties of friction stir butt-welded AA7075 Al alloy plates. Int J Adv Manuf Technol 70, 201-213.

İpekoğlu, G., Erim, S., Çam, G., 2013b. Investigation into the Influence of Post-Weld Heat Treatment on the Friction Stir Welded AA6061 Al-Alloy Plates with Different Temper Conditions. Metallurgical and Materials Transactions A 45, 864-877.

Ji, S., Meng, X., Zeng, Y., Ma, L., Gao, S., 2016. New technique for eliminating keyhole by active-passive filling friction stir repairing. Materials & Design 97, 175-182.

Madhusudhan Reddy, G., Gokhale, A.A., 2014. Chapter 9 - Welding Aspects of Aluminum–Lithium Alloys, Aluminum-lithium Alloys. Butterworth-Heinemann, Boston, pp. 259-302.

Pieta, G., dos Santos, J., Strohaecker, T.R., Clarke, T., 2014. Optimization of Friction Spot Welding Process Parameters for AA2198-T8 Sheets. Materials and Manufacturing Processes 29, 934-940.

Reimann, M., Gartner, T., Suhuddin, U., Göbel, J., dos Santos, J.F., 2016. Keyhole closure using friction spot welding in aluminum alloy 6061–T6. Journal of Materials Processing Technology 237, 12-18.

Sato, Y., Kokawa, H., Enomoto, M., Jogan, S., 1999. Microstructural evolution of 6063 aluminum during friction-stir welding. Metallurgical and Materials Transactions A 30, 2429-2437.

Sato, Y.S., Yamashita, F., Sugiura, Y., Park, S.H.C., Kokawa, H., 2004. FIB-assisted TEM study of an oxide array in the root of a friction stir welded aluminium alloy. Scripta Materialia 50, 365-369.

Shen, Z., Yang, X., Zhang, Z., Cui, L., Li, T., 2013. Microstructure and failure mechanisms of refill friction stir spot welded 7075-T6 aluminum alloy joints. Materials & Design 44, 476-486.

Su, P., Gerlich, A., North, T.H., Bendzsak, G.J., 2006. Energy utilisation and generation during friction stir spot welding. Science and Technology of Welding and Joining 11, 163-169.

Wang, F.F., Li, W.Y., Shen, J., Hu, S.Y., dos Santos, J.F., 2015. Effect of tool rotational speed on the microstructure and mechanical properties of bobbin tool friction stir welding of Al–Li alloy. Materials & Design 86, 933-940.

Zhang, S.-f., Zeng, W.-d., Yang, W.-h., Shi, C.-l., Wang, H.-j., 2014. Ageing response of a Al–Cu–Li 2198 alloy. Materials & Design 63, 368-374.

Zhou, L., Liu, D., Nakata, K., Tsumura, T., Fujii, H., Ikeuchi, K., Michishita, Y., Fujiya, Y., Morimoto, M., 2012. New technique of self-refilling friction stir welding to repair keyhole. Science and Technology of Welding and Joining 17, 649-655.